Progress In Electromagnetics Research, Vol. 142, 591–613, 2013

MINIATURIZED 0.3–6 GHz LTCC SIX-PORT RECEIVER FOR SOFTWARE DEFINED RADIO

Cristina de la Morena-Álvarez-Palencia*, Mateo Burgos-García, and Javier Gismero-Menoyo

Department of Signals, Systems and Radiocommunications, Microwave and Radar Group, Technical University of Madrid, Madrid 28040, Spain

Abstract—The six-port architecture reemerges from the search of low-cost, multi-band and multi-standard transceivers. Its inherent advantages, especially its broadband behavior, make this a structure a good candidate to implement a Software Defined Radio (SDR). However, broadband six-port network designs lead to large size circuits, especially for operating frequencies in the lower gigahertz region. New technologies must be explored in order to achieve compact size and low-cost productions for configurable radio terminals and mobile communication applications. In this paper, the Low Temperature Co-fired Ceramic (LTCC) technology is proposed for implementing a broadband six-port receiver. A compact (30 mm × 30 mm × 1.25 mm) four-octave LTCC six-port receiver is presented. Experimental demodulation results show a good performance over the frequency range from 0.3 to 6 GHz. The demodulation of up to 15.625 Msymbol/s signals, i.e., 93.6 Mbps for 64-QAM, has been satisfactorily performed, with a measured Error Vector Magnitude (EVM) value of 3.7%.

1. INTRODUCTION

Six-port network is an interesting radiofrequency (RF) architecture that is nowadays emerging as a promising alternative for the implementation of a SDR [1–3], as it presents significant advantages with respect to conventional receiver architectures [4, 5]. Six-port architecture has been demonstrated to operate at high frequencies [3] and to perform high data rates [6, 7]. The main advantage of the six-port architecture is its extremely large bandwidth, which involves

Received 8 July 2013, Accepted 15 August 2013, Scheduled 25 September 2013

* Corresponding author: Cristina de la Morena-Álvarez-Palencia (cmorena@gmr.ssr.upm.es).

multi-band and multi-mode capabilities. However, an important problem is the large dimensions of the passive six-port structure.

Six-port configurations are based on the interconnection of several passive circuits, mainly couplers and power dividers. Several examples of six-port network topologies are presented in Figure 1. The bandwidth requirements of a RF front-end for SDR force to use multisection designs, which leads to large size circuits. The higher the frequency, the smaller the passive circuit and the easier the integration in a MMIC (*Monolithic Microwave Integrated Circuit*) design. However, for operating frequencies in the lower gigahertz region, a broadband design in conventional MIC (*Microwave Integrated Circuit*) technology leads to large dimensions, which could be prohibitive, for example, for mobile communication applications. That is the case reported in [7], where a four-octave (0.3–6 GHz) six-port receiver is presented. The six-port network topology is that shown in Figure 1(c), and it is implemented in conventional planar technology [8]. The 90-degree 3-dB couplers are obtained from the tandem connection of two seven section 8.34-dB couplers. The high coupling level of the central section requires the use of broadside-

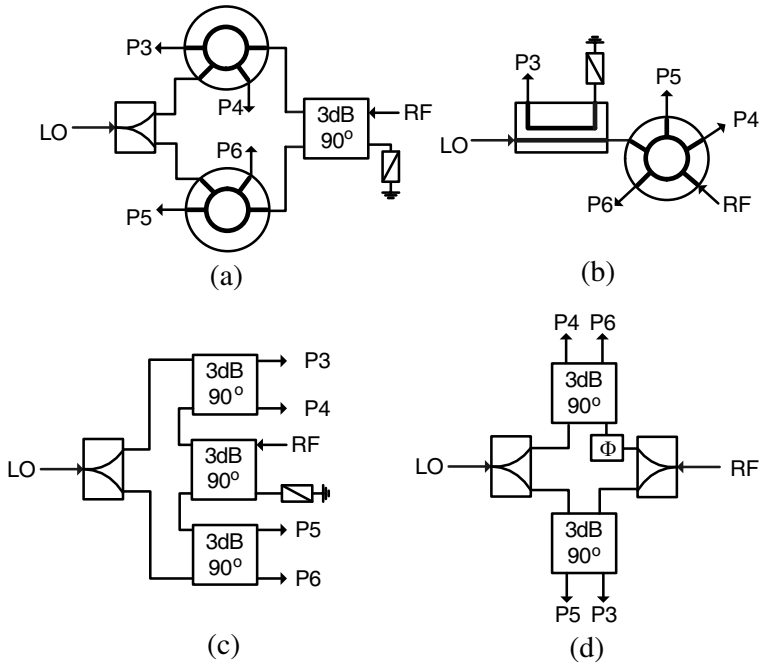

Figure 1. Examples of six-port network topologies.

coupled lines and a low dielectric constant substrate, which increases the size of the circuits even more. The dimensions of the constructed coupler are $130 \times 17 \times 2.6$ mm, and consequently the size of the overall six-port network is not inconsiderable. The six-port demodulation of high-speed signals has been satisfactorily proved from 300 MHz to 6 GHz [7], but some efforts must be made in order to reduce the size.

Therefore, there is a need to explore new technologies in order to make the six-port network a viable and competitive solution for mobile terminals. LTCC is a cost-effective substrate technology which enables to develop compact microwave and millimeter wave modules. It makes possible to integrate passive and active microwave circuits, antenna structures, low-frequency electronics, and digital components on one multilayer substrate. Our objective is to study the contribution of the LTCC technology to the miniaturization of the six-port architecture. Consequently, and continuing our previous work [7, 8], we have developed a new version of the six-port receiver based on LTCC technology. It was briefly mentioned in [5], and now it is presented in this paper in detail.

2. LTCC SIX-PORT RECEIVER DESIGN

The objective is to implement a software configurable receiver prototype, with multi-band and multi-standard capabilities for broadband mobile applications. Nowadays, the aim of a SDR for mobile applications can be reduced to receive every standard up to 6 GHz, approximately, where all cellular and Wireless Local Area Network (WLAN) communications are located. Therefore, the main objective will be to maximize the receiver bandwidth within this frequency range. In addition, the system will be designed to operate with broadband signals, up to 150 MHz-wide signals, and different modulation schemes.

The block diagram of the LTCC six-port receiver is shown in Figure 2. The RF front-end consists of a single LTCC circuit, which is composed of a linear and passive six-port network, four detector diodes, four low-pass filters, four video amplifiers, and four high-pass filters for DC-offset cancellation. The four output signals coming from the six-port receiver, which are baseband signals, are sent to the DSP (digital signal processing) stage, where the six-port calibration and IQ regeneration are performed.

The six-port calibration method will be the channelized auto-calibration method proposed in [7]. It is based on the use of a known training sequence at the beginning of each burst to auto-calibrate the system, as classical real-time multi-port auto-calibration

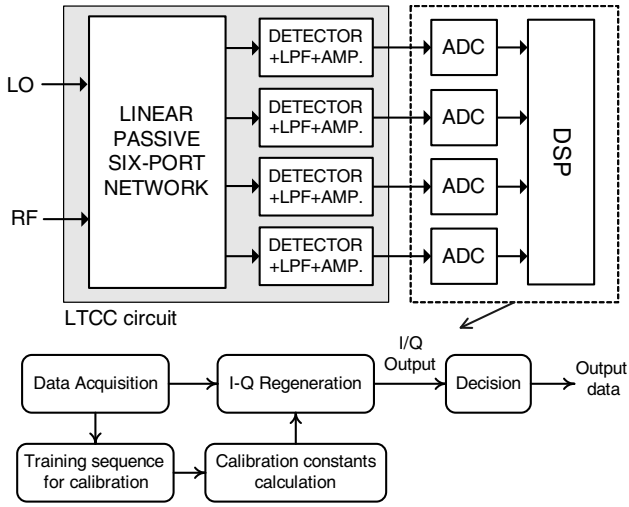

Figure 2. Block diagram of the SDR LTCC six-port receiver.

methods [9, 10]. As novelty, this method proposes a computational efficient digital channelization, with clear benefits for broadband receivers and high data rate applications. The method consists in separating the signal in sub-bands in the digital domain, and calculating the calibration constants at each band separately and simultaneously. The proposed Finite Impulse Response (FIR) filters are easy to implement and have few coefficients, so operations can be real-time performed by the hardware. In addition, operations can be reduced to sums and subtractions using four filters, speeding up the signal processing.

The chosen sixport network topology is that represented in Figure 1(c). This is a typical six-port configuration, formed by three 90-degree hybrid couplers and a Wilkinson power divider, where the RF and LO signals are combined with different relative phase shifts of 0, $\pi/2$, $-\pi/2$, and π rad. The critical element of the six-port network is the 90-degree hybrid coupler, as it determines the system bandwidth. In effect, the greatest difficulty is to design a 3 dB coupler over a very large bandwidth. Branch-line and rate-race couplers are suitable for obtaining tight coupling values, such as 3 dB. However, these couplers are inherently narrowband circuits ($< 20\%$ bandwidth). The use of 3 dB Lange couplers enhances the bandwidth, but only up to one octave. A tight coupler can also be obtained by connecting two couplers in tandem. In a tandem connection, the direct and coupled ports of the first coupler are connected to the isolated and input ports of the

second coupler, respectively. The tandem connection of two 8.34 dB couplers gives rise to a 3 dB coupler. Therefore, a broadband 90-degree hybrid coupler can be obtained from two 8.34 dB multisection couplers.

Consequently, in order to prove the viability and performance of the LTCC technology, we firstly fabricated a stripline three-section 3-dB tandem coupler. We used an LTCC 8-layer DuPont-951 substrate ($\varepsilon_r = 7.8$, tg$\delta = 0.006$@3 GHz). The fabricated circuit was measured with good performance over the frequency range from 1.5 to 6.5 GHz, and a first design version of the LTCC six-port network was proposed [11].

Once the viability of the technology was proved, the design of the complete LTCC six-port receiver was carried out. However, for this second realization, a new substrate with lower loss has been selected: the DuPont-943 ($\varepsilon_r = 7.4$, tg$\delta = 0.001$@3 GHz). DuPont-943 admits narrower layers than DuPont-951 [11], being 42 µm the minimum layer thickness. Then, a wider bandwidth than that obtained with the DuPont-951 substrate could be achieved, since it is determined by the central section coupling level of the 3-dB tandem coupler. The LTCC layer structure is represented in Figure 3.

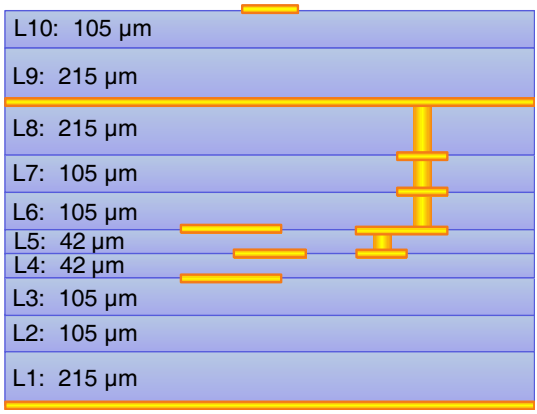

Figure 3. LTCC layer structure, DuPont-943 substrate.

2.1. 3-dB Tandem Coupler

Considering the 934 µm stripline structure composed of layers L1 to L8, the theoretical coupling level that can be achieved with two 50 Ω$\lambda/4$ broadside-coupled striplines separated 84 µm is 4.58 dB. It means that a five-section coupler design could be affordable [12], with the consequent bandwidth increment ($B = f_2/f_1 = 6.35$ for $\delta = 0.35$ dB),

compared with the first fabricated tandem coupler [11]. Nevertheless, with five-section couplers the complete six-port receiver would result in a large size circuit, as three couplers and one power divider must be included.

Alternatively, if the three-section coupler design is maintained, the bandwidth can be extended by increasing the amplitude ripple. For example, a theoretical $B = 4.665$ bandwidth can be obtained for $\delta = 0.55$ dB, leading to a 1254–5850 MHz operating frequency range. In addition, with the new layer structure, the three sections composing the 3-dB coupled lines over layers L3 and L5, avoiding the use of interconnection vias in the previous design [11]. Consequently, we will opt for a three-section coupler design.

The even and odd impedances for a symmetrical 3-section, ± 0.55 dB ripple level, 8.34-dB coupler are compiled in Table 1, together with the coupler dimensions. Figure 4 shows the layout of the LTCC 3-dB tandem coupler, composed of two 8.34-dB couplers connected in tandem. Its simulated frequency response, performed using the EMPIRE XCel 3D-Electromagnetic field simulator from the IMST GMbH, is presented in Figure 5–Figure 6. The simulated input return loss and isolation are better than 20 dB from 0.5 to 6.5 GHz. The simulated insertion loss is 3 ± 0.5 dB from 1.22–5.88 GHz. The amplitude imbalance is below 2 dB from 1 to 6 GHz, while the phase difference between direct and coupled ports varies from 89.8° to 92 between 0.5–6.5 GHz.

Table 1. 3-section 8.34-dB coupler characteristics.

Parameter	Section 1	Section 2
Z_{oe} (Ω)	55.95	91.21
Z_{oo} (Ω)	44.67	27.4
Line width (μm)	250	145
Line spacing (μm)	645	130

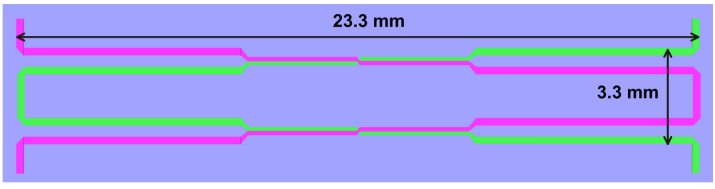

Figure 4. Layout of the LTCC 3-dB tandem coupler.

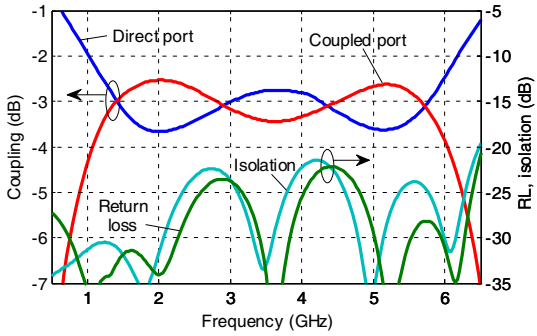

Figure 5. Simulated transmission of the LTCC 3-dB tandem coupler.

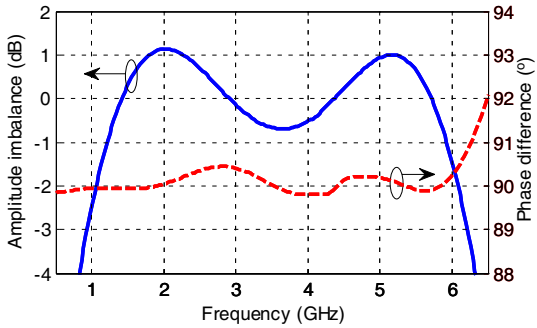

Figure 6. Simulated amplitude and phase imbalances of the LTCC 3-dB tandem coupler.

2.2. Wilkinson Power Divider

A multisection Wilkinson divider design is needed to cover the design frequency range of the 3-dB tandem coupler (1254–5850 MHz). From the design equations [13], and setting an input return loss better than 20 dB, we obtain that three sections are required to cover the operating frequency range. The Wilkinson divider will be implemented in microstrip using layers L1 and L2. The parameters of the 3-section Wilkinson divider are given in Table 2. The layout of the circuit and the EM simulated response (using EMPIRE) are presented in Figure 7 and Figure 8, respectively.

2.3. LTCC Six-port Network

For the design of the six-port network, three 3 dB tandem couplers and a Wilkinson divider have been connected according to the topology of

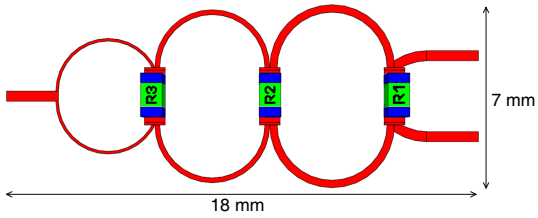

Figure 7. Layout of the Wilkinson power divider.

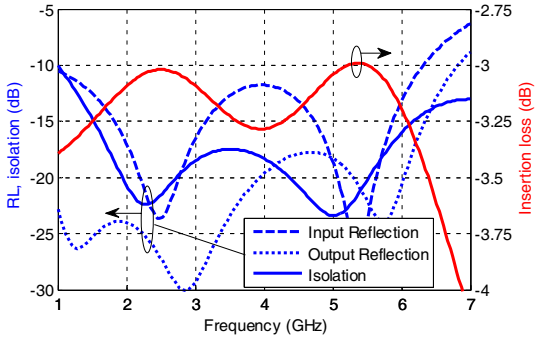

Figure 8. Simulated frequency response of the LTCC Wilkinson divider.

Table 2. 3-section Wilkinson power divider parameters.

Design Parameters	**Section 1**	**Section 2**	**Section 3**
Z_o (Ω)	57.77	70.71	86.54
R (Ω)	371.41	207.66	108.64
Implementation	**Section 1**	**Section 2**	**Section 3**
Line width (μm)	285	185	100
R (Ω)	365	205	100

Figure 1(c). The 3D view the LTCC six-port network, along with the scheme of the circuits' distribution in the layer structure, are presented in Figure 9 (the ground metal located over layers L2 and L8 has been removed in the figure). The inputs and outputs of the six-port network are implemented in microstrip using layers L9 and L10. The interconnection between the different layers will be made by means of vias (175 μm diameter). These vias will be also used to build electrical walls in order to isolate the circuits composing the

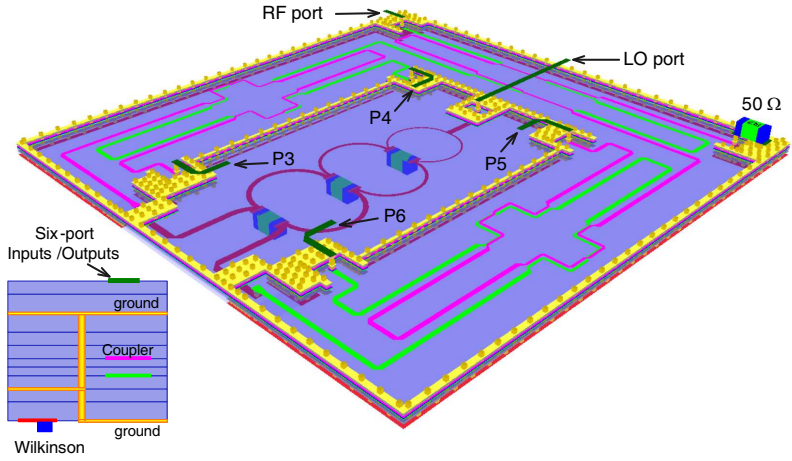

Figure 9. 3D view of the LTCC six-port network.

receiver. The design of a microstrip-to-stripline transition has been required to connect the couplers with the Wilkinson divider and with the outputs. For the interconnection between the LO input port and the Wilkinson divider, a microstrip-to-microstrip transition design has been also developed.

The dimensions of the six-port network are 30 mm × 30 mm × 1.254 mm. Our purpose is to take advantage of the LTCC possibilities to develop a complete LTCC six-port receiver. Then, the free area over the three couplers will be used to locate the four power detectors and the low-frequency components. Furthermore, there is still a central free space above the Wilkinson divider occupying layers L3 to L8.

The EM simulated response of the LTCC six-port network will be presented in Section 3, together with the measurement results.

2.4. Complete LTCC Six-port Receiver

The overall receiver includes a power detector, a low-pass filter and a video amplifier at each six-port network output, implemented in microstrip using the two upper layers L9 and L10.

Our system specifications impose large RF operation frequency range and a wide video bandwidth (75 MHz). Obviously, such a detector will not have high voltage sensitivity, since sensitivity and video bandwidth are competitive parameters. A bias current higher than that required for maximum sensitivity will be needed to achieve

the required video bandwidth. However, it will be advantageous for RF input matching and dynamic range extension. Multiport architectures do not present good behavior as for dynamic range, compared with heterodyne and conventional homodyne receivers. The main reason is that most of the six-port implementations use zero-bias detector diodes, matched at narrow band and/or with small video bandwidth. Consequently, no many experimental six-port demodulation results providing both multiband and high-data rate operation have been published up to now. Therefore, since the maximization of sensitivity will not be possible due to the wide video bandwidth requirement, a high bias current will be selected in order to extend the dynamic range.

The power detectors will be implemented with the HP HSMS-286 Schottky diode, which will be biased with a $I_b = 0.5\,\mathrm{mA}$ bias current. Such a high current will provoke large sensitivity degradation, whereby a video amplifier will be included. A shunt $50\,\Omega$ resistor will be also used to give broadband input match, but at the expense of detection sensitivity.

MiniCircuits LFCV-45+ (77 MHz cut-off frequency) and MAR-8A+ components will be used for the low-pass filters and video amplifiers, respectively. The low noise amplifier (LNA) and the automatic gain control (AGC) stage have not been included in the prototype, although these components would be necessary in a SDR front-end. Another important issue in a SDR implementation is the RF filtering to eliminate the out-of-band interference signals. But multi-band or tuneable RF filters are difficult to design over large frequency ranges. Conventional multi-band filtering techniques have consisted of filter banks, with the disadvantage of the circuit size. More advanced techniques are based on single circuits performing the multi-band filtering. Many solutions of dual-, triple- or quad-band have been proposed, and currently the efforts are focused on the design of multi-band filters with an arbitrary number of pass-bands. Moreover, micro-electromechanical systems (MEMS) devices have displayed remarkable characteristics as variable devices and have been applied as tuneable or reconfigurable multi-band RF circuits. Anyway, the multi-band frequency-selective filtering is a wide research area and it would deserve a separate investigation, which is far from the objective of this work.

The 3D view of the final LTCC six-port receiver is represented in Figure 10. The distribution scheme of the six-port receiver components can be seen in Figure 11. The dimensions of the LTCC six-port receiver are $30\,\mathrm{mm} \times 30\,\mathrm{mm} \times 1.254\,\mathrm{mm}$. It is worth to mention that there is a free area of $238\,\mathrm{mm}^2$ above the Wilkinson divider in layers L3–L8, which may still be occupied. One of the possibilities could be, for example, to locate a RF filter.

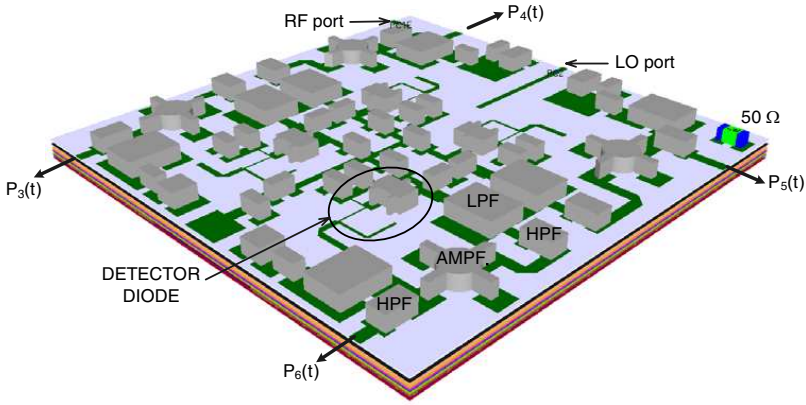

Figure 10. 3D view of the LTCC six-port receiver (top).

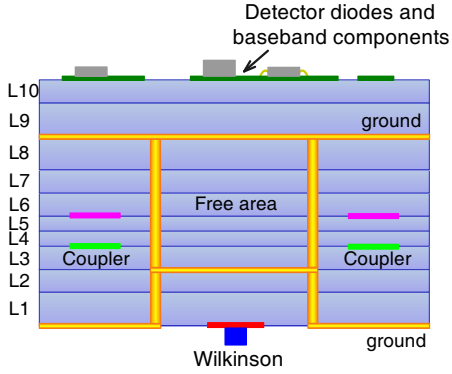

Figure 11. Distribution of the circuits in the 10 layer LTCC structure.

3. IMPLEMENTATION AND EXPERIMENTAL CHARACTERIZATION

Completed the LTCC six-port receiver design, the circuit was fabricated by the IMST GMbH. The photograph of the fabricated LTCC circuit is shown in Figure 12.

Firstly, the scattering parameters of the LTCC six-port network will be measured. The measurement has been performed using a probe station, as shown in Figure 13. The development of a test-platform composed of a metallic test-box and two access circuits has been required for the measurement, which can be seen in Figure 13. In addition, the four output microstrip lines of the six-port network have

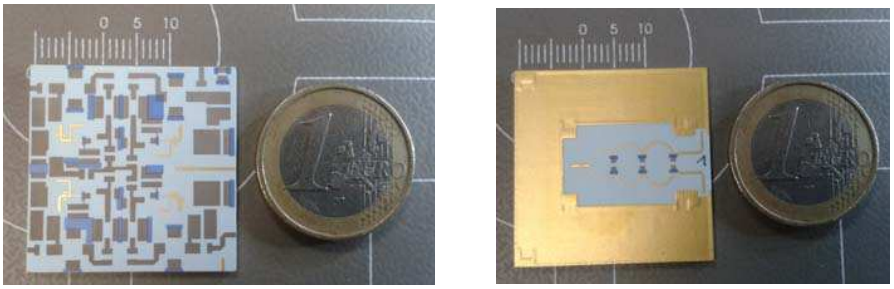

(a) (b)

Figure 12. Fabricated LTCC six-port receiver. (a) Top view. (b) Bottom view.

Figure 13. Test-bench for the measurement of the scattering parameters.

Figure 14. Detail of one output port with ground patches for probe positioning.

not been joined to the detector diodes, and two ground patches have been placed at every output port for probe positioning. The detail of one output port can be seen in Figure 14. Once the six-port network measurement has been made, the four output lines will be joined to the detector diodes. For this first measurement, only the 50 Ω resistor and the Wilkinson resistors need to be soldered.

The responses of the additional elements required for the measurement, such as microstrip access circuits, probes, etc., have been removed by means of deembedding techniques. Figure 15 shows the simulated and measured return loss and isolation of the six-port network. The measured return loss at the LO port, which is conditioned by the Wilkinson input reflection, is in accordance with the simulation results, with a value below 10 dB from 1 GHz to 6 GHz. On the contrary, the measured return loss at RF port differs from the simulations, with worse values than expected. This could be due to

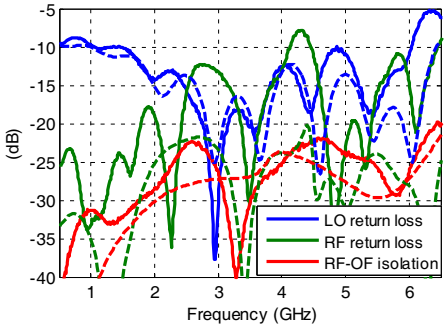

Figure 15. Measured (solid line) and simulated (dashed line) input return loss and isolation.

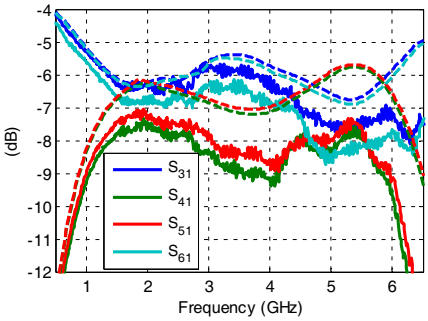

Figure 16. Measured (solid line) and simulated (dashed line) attenuations from the LO port.

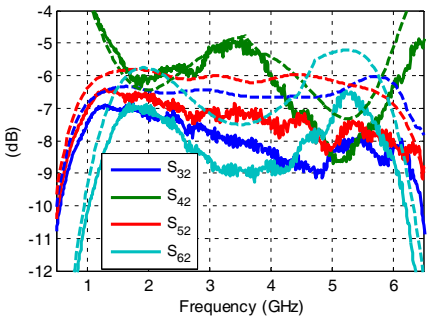

Figure 17. Measured (solid line) and simulated (dashed line) attenuations from the RF port.

imperfections in the junction with the microstrip access circuit of the test platform, or in the LTCC microstrip-to-stripline transition. As for the measured RF-LO isolation, it is better than 20 dB up to 6.5 GHz.

Figure 16 and Figure 17 present, respectively, the simulated and measured attenuations from the LO and the RF ports. The simulated and measured curves present the same tendency, although additional losses are observed in the coupling levels, which can vary from 1 dB to 2 dB. This was expected, as an additional 0.8 dB loss in the coupling level of the fabricated 3 dB tandem coupler was already observed in [11]. Anyway, what is important is to maintain a good distribution of the q_i-points. Ideally, in this six-port topology the magnitudes of q_i-points are equal to 1, and the arguments differ 90 degrees. Figure 18(a) shows the simulated and measured magnitudes of the q_i-points, while the phases with respect to port 3 are plotted in Figure 18(b). The

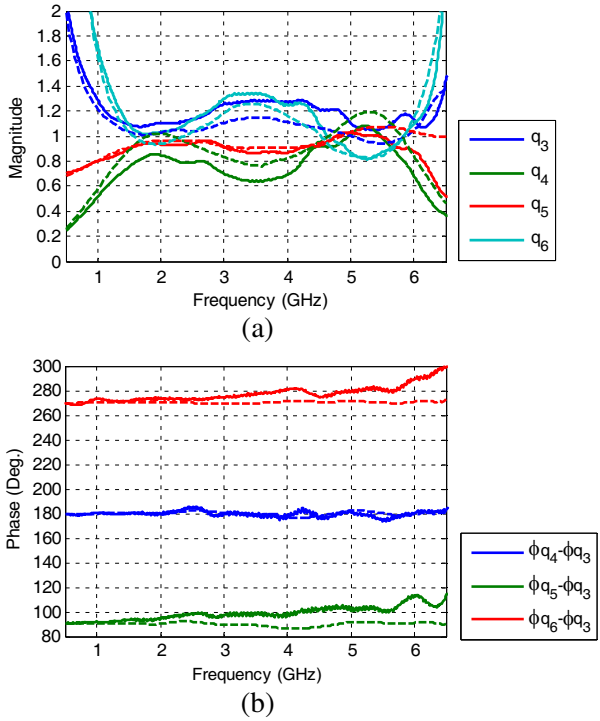

Figure 18. Measured (solid line) and simulated (dashed line) q_i-points: (a) Magnitude. (b) Arguments.

measured magnitudes of q_i are in the range of 0.5 to 1.8 from 1 GHz to 6 GHz. The behavior of the curves below 1 GHz and above 6 GHz show that the operation range of the LTCC six-port receiver may be enlarged, as it happened with the first developed six-port receiver prototype [7, 8]. Regarding to the phase of the q_i-points, the maximum error in the relative phase differences is 20° over the theoretical value below 6 GHz. This value may seem quite high. However, take into account that small positioning errors in the probes provoke significant phase errors at high frequencies. In any case, this deviation will be compensated by the calibration algorithm, as it will be seen in Section 4.

Finally, after measuring the six-port network scattering parameters, the rest of the components were soldered to the LTCC circuit. The circuit was introduced into a metallic box, resulting in the final LTCC six-port receiver prototype. Its photograph can be seen in Figure 19.

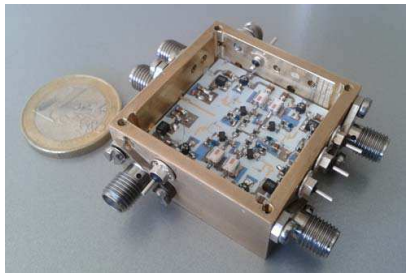

Figure 19. Fabricated LTCC six-port receiver prototype.

4. DEMODULATION RESULTS

Finally, the demodulation capability of the fabricated LTCC six-port receiver will be evaluated. The scheme of the test-bench is shown in Figure 20. The *Agilent* E4438C ESG and N5182A MXG Vector Signal Generators (VSG) will be used for generating the RF modulated signal. The LO will be generated by the *Agilent* synthesized sweeper 83752A. The LO and RF signal generators will be phase locked. The output signals of the six-port receiver will be acquired by a four-channel oscilloscope (*Agilent Infiniium*), with an over-sampling ratio OSR = 8. The software containing the channelized auto-calibration method (AM), implemented in *Matlab,* will be applied in a personal computer. The software does not include any diode linearization technique. It is worth to mention that the maximum symbol rate that

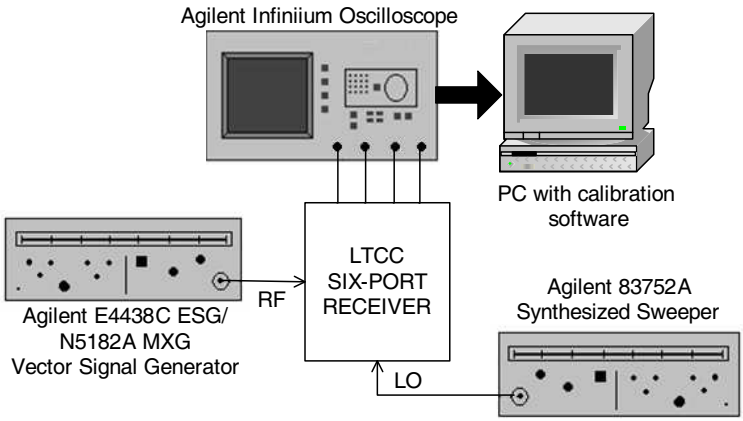

Figure 20. Set-up of the LTCC six-port receiver test-bench.

can be obtained with the E4438C ESG VSG is 12.5 Msymbol/s for an OSR = 8. The *Agilent* N5182A MXG can provide 15.625 Msymbol/s for OSR = 8, but it only operates up to 3 GHz. However, from the 3 dB cut-off frequency of the low-pass filter, 154 Msymbol/s could be performed, that is, 924 Mbps for 64-QAM.

The LO power will be set to $P_{LO} = 0$ dBm. After the acquisition of 1000 symbols (8000 samples, OSR = 8), the data will be processed as bursts of length 200 symbols. The first 50 symbols of each burst will be used to auto-calibrate the system, and then the data sequence of length 150 symbols will be demodulated. The quality of the demodulated signal will be evaluated in terms of EVM.

Figure 21 shows the received constellation diagrams at 2.4 GHz and 15.625 Msymbol/s for different modulation schemes: 64-QAM, 16-QAM and QPSK. The power level of the RF modulated signal, P_{in}, is -25 dBm. The results show a good performance of the LTCC six-port receiver. The measured EVM is around 3.7% for the three cases (using the channelized AM, downsampling with a ratio of 2, and four FIR filters [7]).

Figure 22 presents the measured EVM as a function of the frequency. In this case, a -20 dBm 64-QAM signal at 12.5 Msymbols/s, i.e., data rate 75 Mbps, has been demodulated. We have plotted the EVM curves obtained from the conventional AM [9, 10], with no sub-band division, and from the channelized AM [7] with different number of FIR filters, N. The results show significant EVM improvements with respect to the conventional AM: up to 0.5 percentage points for

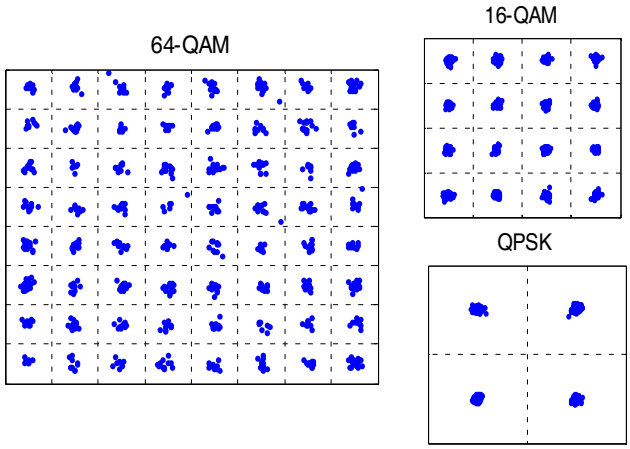

Figure 21. Received constellations: 15.625 Msymbol/s, $P_{LO} = 0$ dBm, $P_{in} = -25$ dBm.

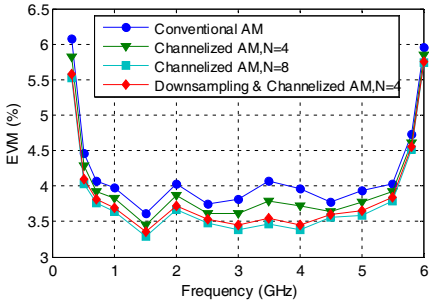

Figure 22. Measured EVM versus frequency: 75 Mbps 64-QAM, $P_{LO} = 0$ dBm, $P_{in} = -20$ dBm.

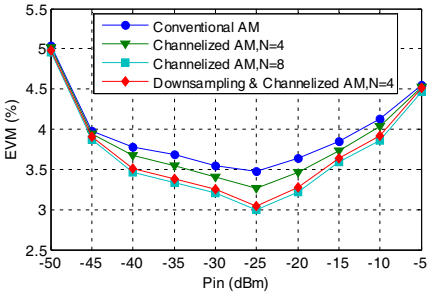

Figure 23. Measured EVM versus P_{in}: 75 Mbps 64-QAM, $P_{LO} = 0$ dBm, $f = 2.5$ GHz.

$N = 8$ filters, or $N = 4$ with downsampling (factor 2). The advantage of using four filters is that the I-Q regeneration operations reduce to sums and subtractions [7], speeding up the signal processing. Then, by using the channelized AM with downsampling and $N = 4$, the measured EVM is below 3.8% from 700 MHz to 5.5 GHz. Moreover, the demodulation results demonstrate that the operating range of the LTCC six-port receiver can be extended from 300 MHz to 6 GHz (4.32 octaves) with good performance, as it was expected. The measured EVM is below 5.75% from 300 MHz to 6 GHz.

Figure 23 shows the measured EVM as a function of P_{in} at 2.5 GHz. Note that in this case the EVM/BER improvement due to the use of the proposed channelized AM is more significant than in the first developed six-port receiver [7], as the variation of the six-port parameters with frequency is stronger. EVM curves show quality degradation for high levels of P_{in} due to nonlinear behavior of the diodes and to the rectified wave, a baseband term superposed to the desired signal that increases quadratically with the signal power and, therefore, produces more degradation for high power levels.

For a Gaussian noise model and a number of received symbols greater than the alphabet length, EVM and signal to noise ratio (SNR) are related by the expression

$$\mathrm{SNR} = \frac{1}{\mathrm{EVM}^2} \tag{1}$$

Figure 24 presents the corresponding BER (Bit Error Rate) curves calculated from the measured EVM using (1). By defining the sensitivity as the RF input power to ensure a BER of 10^{-3}, we obtain a sensitivity value of -56.5 dBm at 2.5 GHz. Take into account that

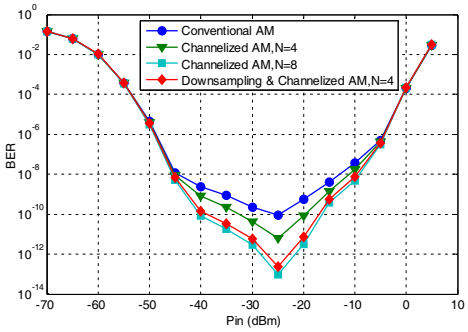

Figure 24. BER calculated from measured EVM: 75 Mbps 64-QAM, $P_{LO} = 0\,\text{dBm}$, $f = 2.5\,\text{GHz}$.

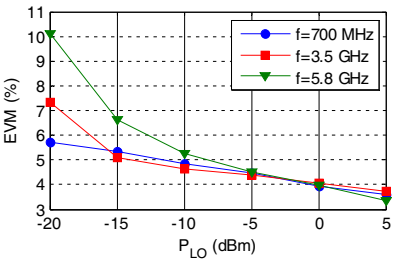

Figure 25. Measured EVM versus PLO: 25 Mbps QPSK, $P_{in} = -20\,\text{dBm}$.

the LNA and the AGC stages have not been included in the prototype. Moreover, the dynamic range is 58 dB at BER $\leq 10^{-3}$. This is a high dynamic range compared with six-port receivers based on zero-biased detector diodes. For example, a 37.3 dB dynamic range at 2.4 GHz is measured in [14], despite that the response of the detectors has been linearised using software techniques. On the contrary, we do not use any diode linearization technique.

Finally, the EVM has been measured for different LO power levels. Figure 25 presents the measured EVM at 700 MHz, 3.5 GHz, and 5.8 GHz, using the channelized AM method with down sampling and four FIR filters. These results clearly demonstrate the capacity of the six-port receiver to operate with low values of LO power. This is an important advantage for SDR, as it entails low power consumption and cost reduction. In addition, problems derived from LO leakage and the self-mixing of LO, which are major drawbacks in direct conversion architectures, can be reduced.

4.1. Comparison of Multi-port Demodulators

To conclude, the comparison with other multi-port demodulators operating in the frequency range of interest is presented in Table 3. As the quality of the demodulated signal is evaluated in terms of EVM or BER, we provide the theoretical BER versus EVM curves for QPSK, 16-QAM, and 64-QAM modulation schemes in Figure 26.

Although the six-port receiver is said to be a good solution for the multi-band demodulation of high-speed signals, no many experimental demodulation results proving both assumptions have been published up to now. Some published works are not strictly multi-

band [10, 18]; other are multi-band, but only validate the demodulator for a single frequency [17, 19]; and other prove the multi-band behavior, but do not quantify the quality of the demodulated signal [16].

Table 3. Comparison of multi-port demodulators.

Ref.	**Operating freq. band (GHz)**	**Measurement results**				
		Data signal	**P_{LO} (dBm)**	**P_{in} (dBm)**	**Freq. (GHz)**	**Quality of demodulated signal**
[15] (2003)	0.9–5	97.2 Kbps QPSK	0	−20	0.9–4	EVM < 14%
[10] (2004)	2–3	200 Kbps QPSK	0	−62.5	2	BER = 10^{-3}
[16] (2006)	2–9.4	8PSK	-	−19	2.4	Not quantified
				−27	5.8	
				−31	9.4	
[17] (2006)	0.9–4	1 Mbps QPSK	−10	−15	2.45	EVM = 12%
[18] (2008)	3.1–4.8	1 Mbps QPSK	−1.5	-	3.432	EVM = 5.5%
					3.96	EVM = 4%
					4.488	EVM = 6.3%
[14] (2009)	0.8–2.4	4 Mbps 16QAM	−8.5	−33.3 to −2.6	0.8	BER < 10^{-3}
				−39.6 to −0.6	1.6	
				−38 to −0.7	2.4	
				≈ −32	1.6	BER = 10^{-6}
[19] (2010)	0.9–4	400 Kbps QPSK	−10	−20	2.45	EVM = 5.9%
				−40		EVM = 7.9%
[6] (2010)	7–8	1.67 Gbps 16-QAM	15	−15	7.5	EVM = 10.9%
[7] (2011)	0.3–6	75 Mbps 64-QAM	0	−20	0.3	EVM = 6.1%
		62.5 Mbps 16-QAM			0.7	EVM = 4.8%
		93.75 Mbps 64-QAM			2.45	EVM = 4.5%
		25 Mbps QPSK			6	EVM = 4.4%
		25 Mbps QPSK	−20	−20	1.8	EVM = 6.3%

This work (2013)	0.3–6	75 Mbps 64-QAM	0	−20	0.7–5.5 0.3–6	EVM < 3.8% EVM < 5.75%
				−56.5 to 1.5	2.5	BER < 10^{-3}
		25 Mbps QPSK	−20 to +5	−20	0.7 3.5 5.8	EVM 5.75–3.6% 7.3–3.7% 10.1–3.3%
		15.625 Msymbol/s 64-QAM 16-QAM QPSK	0	−25	2.4	EVM = 3.7%

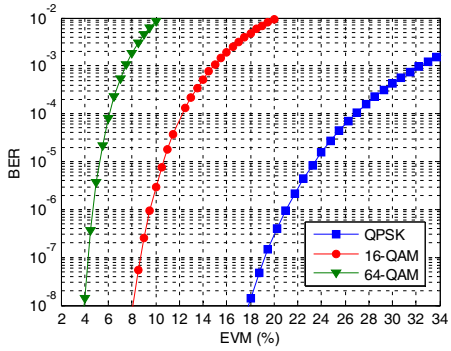

Figure 26. Theoretical BER versus EVM curves.

In [14, 15] the demodulation performance is quantified over the entire operating frequency range, but with data rates much lower than in our experiments. A six-port demodulator supporting a 1.67 Gbps data rate was published in [6]. However, this is not a broadband design, as it only covers the range from 7 to 8 GHz. In addition, the measured EVM is quite high, even though the high LO power level (15 dBm). The six-port receiver presented in [7], and the LTCC six-port receiver presented in this paper outperform the other multiport receivers in terms of bandwidth, dynamic range, and quality of the demodulated signal. They have been validated over a four octave bandwidth (0.3–6 GHz), and for up to 93.75 Mbps data rates with very low values of EVM. Moreover, the proposed LTCC six-port receiver not only outperforms the other receivers in these aspects, but also in terms of size: $30 \times 30 \times 1.25$ mm. Other multilayer [20–22] or miniaturized microstrip [23] six-port designs have appeared in

the literature. Nonetheless, they do achieve neither such a reduced size nor such large frequency range than the proposed LTCC six-port receiver. In addition, these publications do not provide any experimental demodulation results.

5. CONCLUSION

A compact 0.3–6 GHz LTCC six-port receiver for SDR has been presented in this paper. Due to the use of the LTCC technology, the dimensions of the six-port receiver have been reduced to $30 \times 30 \times 1.25$ mm. This work demonstrates empirically and quantitatively the multi-band behavior of the six-port architecture, and the capability of performing high data rates. The demodulation of up to 15.625 Msymbol/s signals, i.e., 93.6 Mbps for 64-QAM, has been satisfactorily performed, with lower values of EVM than those published before in the literature. These promising results may lead to reconsider the six-port architecture as an alternative for the lower gigahertz region, hence for mobile communication applications. Furthermore, an important enhancement of the six-port receiver dynamic range has been achieved due to the use of biased detector diodes. It is worth to mention that we do not to use any digital diode linearization technique, which would extend the dynamic range for high power levels.

ACKNOWLEDGMENT

This work was supported by the Spanish National Board of Scientific and Technological Research (CICYT), under project contracts TEC2008-02148, and TEC2011-28683-C02-01.

REFERENCES

1. Mohaer, M., A. Mohammadi, and A. Adipour, "Direct conversion receivers using multi-port structures for software defined radio systems," *IET Microw. Antennas & Propag.*, Vol. 1, No. 2, 363–372, Apr. 2007.
2. Bosisio, R. G., Y. Y. Zhao, X. Y. Xu, S. Abielmona, E. Moldovan, Y. S. Xu, M. Bozzi, S. O. Tatu, C. Nerguizian, J. F. Frigon, C. Caloz, and K. Wu, "New-wave radio," *IEEE Microw. Magazine*, Vol. 9, No. 1, 89–100, 2008.
3. Koelpin, A., G. Vinci, B. Laemmle, D. Kissinger, and R. Weigel, "The six-port in modern society," *IEEE Microw. Magazine*, Vol. 11, No. 7, 35–43, Dec. 2010.

4. Khaddaj Mallat, N., E. Moldovan, and S. O. Tatu, "Comparative demodulation results for six-port and conventional 60 GHz direct conversion receivers," *Progress In Electromagnetics Research*, Vol. 84, 437–449, 2008.
5. De la Morena-Álvarez-Palencia, C. and M. Burgos-Garcia, "Experimental performance comparison of six-port and conventional zero-IF/low-IF receivers for software defined radio," *Progress In Electromagnetics Research B*, Vol. 42, 311–333, 2012.
6. Östh, J., A. Serban, Owais, M. Karlsson, S. Gong, J. Haartsen, and P. Karlsson, "Six-port gigabit demodulator," *IEEE Trans. Microwave Theory Tech.*, Vol. 59, No. 1, 125–131, Jan. 2010.
7. De la Morena-Álvarez-Palencia, C. and M. Burgos-García, "Four-octave six-port receiver and its calibration for broadband communications and software defined radios," *Progress In Electromagnetics Research*, Vol. 116, 1–21, 2011.
8. De la Morena-Álvarez-Palencia, C., M. Burgos-García, and D. Rodríguez-Aparicio, "Three octave six-port network for a broadband software radio receiver," *European Microwave Conf.*, 1110–1113, Paris, France, 2010.
9. Xu, Y. and R. G. Bosisio, "On the real time calibration of six-port receivers (SPRs)," *Microw. Opt. Technol. Lett.*, Vol. 20, No. 5, 318–322, 1999.
10. Neveux, G., B. Huyart, and G. J. Rodriguez-Guisantes, "Wideband RF receiver using the 'five-port' technology," *IEEE Trans. Vehicular Technology*, Vol. 53, No. 5, 1441–1451, Sep. 2004.
11. De la Morena-Álvarez-Palencia, C., M. Burgos, and J. Gismero-Menoyo, "Contribution of LTCC technology to the miniaturization of six-port networks," *European Microw. Conf.*, 659–662, Manchester, UK, Oct. 2011.
12. Cristal, E. G. and L. Young, "Theory and tables of optimum symmetrical TEM-mode coupled-transmission-line directional couplers," *IEEE Trans. Microwave Theory Tech.*, Vol. 13, 544–558, Sep. 1965.
13. Cohn, S. B., "A class of broadband three-port TEM mode hybrids," *IEEE Trans. Microw. Theory Tech.*, Vol. 16, No. 3, 110–116, Feb. 1968.
14. Perez-Lara, P., J. A. Medina-Rodriguez, I. Molina-Fernandez, J. G. Wanguemert-Perez, and A. Gonzalez-Salguero, "Wideband homodyne six-port receiver with high LO-RF isolation," *IET Microw. Antennas Propag.*, Vol. 3, No. 5, 882–888, 2009.

15. Xiong, X. Z. and V. F. Fusco, "Wideband 0.9 GHz to 5 GHz six-port and its application as digital modulation receiver," *IET Microw. Antennas Propag.*, Vol. 150, No. 4, 301–307, Aug. 2003.
16. Tatu, S. O., K. Wu, and T. Denidni, "Multiband multiport direct conversion receiver: Design, implementation and demodulation results," *Microw. Optical Technology Lett.*, Vol. 48, No. 4, 817–822, Apr. 2006.
17. Haddadi, K., H. El Aabbaoui, C. Loyez, D. Glay, N. Rolland, and T. Lasri, "Wide-band 0.9 GHz to 4 GHz four-port receiver," *IEEE Int. Conf. Electron. Circuits and Systems*, 1316–1319, Nice, France, Dec. 2006.
18. Hakansson, P. and S. Gong, "Ultra-wideband six-port transmitter and receiver pair 3.1–4.8 GHz," *Asia-Pacific Microw. Conf.*, 1–4, Hong Khong/Macau, China, Dec. 2008.
19. Haddadi, K., M. M. Wang, C. Loyez, D. Glay, and T. Lasri, "Four-port communication receiver with digital IQ-regeneration," *IEEE Microw. Wireless Compon. Lett.*, Vol. 20, No. 1, 58–60, Jan. 2010.
20. Winter, S. M., A. Koelpin, and R. Weigel, "Six-port receiver analog front-end: Multilayer design and system simulation," *IEEE Trans. Circuits Sist. II*, Vol. 55, No. 3, 254–258, Mar. 2008.
21. Moscoso-Martir, A. and I. Molina-Fernandez, "Six-port junction with complete UWB band coverage in multilayer technology," *European Microwave Conf.,* 655–658, Manchester, UK, Oct. 2011.
22. Peng, H., Z. Yang, and T. Yang, "Design and implementation of an ultra-wideband six-port network," *Progress In Electromagnetics Research*, Vol. 131, 293–310, 2012.
23. Fang, X. T., X.-C. Zhang, and C.-M. Tong, "A novel miniaturized microstrip six-port junction," *Progress In Electromagnetics Research Letters*, Vol. 23, 129–135, 2011.